Rock and Soil Mechanics

Volume 44 | Issue 5 Article 4

8-21-2023

Applicability of power-law stress-strain model for coral sand under earth fills stress path

Ji-ru ZHANG
School of Civil Engineering and Architecture, Wuhan University of Technology, Wuhan, Hubei 430070, China

Yan-jun ZHENG
School of Civil Engineering and Architecture, Wuhan University of Technology, Wuhan, Hubei 430070, China

Wei-ke PENG
School of Civil Engineering and Architecture, Wuhan University of Technology, Wuhan, Hubei 430070, China

Lei WANG
School of Civil Engineering and Architecture, Wuhan University of Technology, Wuhan, Hubei 430070, China

See next page for additional authors

Follow this and additional works at: https://rocksoilmech.researchcommons.org/journal

 Part of the Geotechnical Engineering Commons

Recommended Citation

ZHANG, Ji-ru; ZHENG, Yan-jun; PENG, Wei-ke; WANG, Lei; and CHEN, Jing-xin (2023) "Applicability of power-law stress-strain model for coral sand under earth fills stress path," *Rock and Soil Mechanics*: Vol. 44: Iss. 5, Article 4.
DOI: 10.16285/j.rsm.2022.5953
Available at: https://rocksoilmech.researchcommons.org/journal/vol44/iss5/4

This Article is brought to you for free and open access by Rock and Soil Mechanics. It has been accepted for inclusion in Rock and Soil Mechanics by an authorized editor of Rock and Soil Mechanics.

Applicability of power-law stress-strain model for coral sand under earth fills stress path

Authors

Ji-ru ZHANG, Yan-jun ZHENG, Wei-ke PENG, Lei WANG, and Jing-xin CHEN

This article is available in Rock and Soil Mechanics: https://rocksoilmech.researchcommons.org/journal/vol44/iss5/4

Rock and Soil Mechanics 2023 44(5): 1309−1318 ISSN 1000−7598
https: //doi.org/10.16285/j.rsm.2022.5953 http://rocksoilmech.researchcommons.org/journal

Applicability of power-law stress-strain model for coral sand under earth fills stress path

ZHANG Ji-ru, ZHENG Yan-jun, PENG Wei-ke, WANG Lei, CHEN Jing-xin
School of Civil Engineering and Architecture, Wuhan University of Technology, Wuhan, Hubei 430070, China

Abstract: Coral sands are commonly used in hydraulic fill foundations and as subgrade fill in the construction of islands and reefs. The stress paths followed by soil consolidation or filled subgrade are characterized by K_0 consolidation or constant stress ratio stress path. It is necessary to develop a computational model that reflects the effect of stress path on deformation in order to accurately estimate soil deformation during the filling process. Based on the generalized Hooke's law, a nonlinear elastic model in the form of a power function is proposed to describe the stress-strain curve of coral sand, and the functional expression is given. A series of K_0 consolidation tests and drained triaxial compression tests with a constant stress ratio path were conducted on the coral sand to investigate the stress-strain curves and the behavior of particle breakage. The applicability of the power-law stress-strain model for the coral sand under the earth fill stress path was investigated, and the calculated results of the model were compared with the test curves. The results show that the stress-strain curves under both K_0 consolidation and constant stress ratio paths conform to the form of power-law curves and can be described by a power-law nonlinear elastic model. The tangent modulus and tangent Poisson's ratio of this model can be expressed as a function of axial effective stress and can be determined by parameters related to the stress increment ratio or K_0 coefficient. Under a constant stress ratio path, the tangent Poisson's ratio and tangent modulus increase with the increase of the axial effective stress. For the same axial effective stress condition, a large stress ratio corresponds to a large tangent modulus and a small tangent Poisson's ratio. With the increase of the axial effective stress under the condition of K_0 consolidation, the coefficient of earth pressure at rest and tangent Poisson's ratio decrease, while the tangent modulus increases. Under the stress paths of K_0 consolidation and constant stress ratio, the amount of particle breakage of coral sand within the test stress range is very small and therefore has little effect on the stress-strain curve. Under the constant stress ratio path, the stress-strain curve of coral sand in a certain stress ratio range can be reasonably predicted by the power function model, in which the effects of different constant stress ratio paths on the stress-strain relationship are considered.

Keywords: power-law stress-strain model; triaxial stress path test; coral sand; constant stress ratio path; K_0 consolidation

1 Introduction

Coral islands and reefs are generally far from the mainland. Thus, the construction of the islands and reefs can only depend on local materials. Coral reef sediments are commonly used to fill the ground[1–3], or as fillers for geotechnical structures such as subgrade and retaining walls[4–5]. These sediments are mainly coral sand with the characteristics of easily broken particles, rich internal pores, and irregular shapes. At present, coral reef sediments are not included in the filler of the relevant foundation survey and design codes. Therefore, it is necessary and beneficial to carry out application research on coral reef sand ground engineering.

Acceptance of the fill construction of the hydraulic fill ground or geotechnical structures needs to meet the engineering design elevation. Since the drainage consolidation of the filling soil will produce a large settlement deformation, it is necessary to reserve a certain height during construction to ensure project quality and control construction cost. Thus, it is particularly important to accurately predict the soil settlement during the filling period. The earthfill stress path refers to the stress path of the soil filling during the ground consolidation or filling period. The stress path during the consolidation period of reclaimed ground approximates K_0 consolidation (coefficient K_0 of earth pressure at rest is the ratio of horizontal to vertical effective principal stresses in soil under the unconfined lateral deformation condition, which is a basic parameter of soil mechanics). The stress path during the filling period of geotechnical structures is characterized by the constant stress ratio path and the principal stress increment ratio varies with the filling location[6]. Since the stress-strain relationship of sand has obvious stress path dependence characteristics[7], for the deformation prediction of coral sand during the filling period, it is necessary to establish a simple and practical calculation model that can consider the influence of the actual stress path, to improve the design and construction quality of island projects.

Soil is a loose aggregate of particles, and its stress–strain relationship has obvious nonlinear characteristics. Among the stress–strain models of soil, the elastoplastic model and the nonlinear elastic model are the two main constitutive models. Among them, the elastoplastic model better reflects the deformation characteristics and hardening, softening and dilatancy properties of soil, such as the Cambridge model proposed by Roscoe et al.[8–9] and the Lade-Duncan

Received: 22 June 2022 Accepted: 8 August 2022
This work was supported by the National Natural Science Foundation of China (42172295).
First author: ZHANG Ji-ru, male, born in 1964, PhD, Professor, PhD supervisor, mainly engaged in teaching and research in geotechnical engineering. E-mail: zhangjr@whut.edu.cn

model proposed by Lade et al.[10]. However, these models are generally more complex and the parameters are relatively difficult to be obtained. The nonlinear elastic model can describe the nonlinear characteristics of soil, and at the same time have the characteristics of the simple form and few parameters, such as, the hyperbolic elastic modulus-Poisson's ratio model proposed by Duncan et al.[11−12] and the subsequent improved elastic modulus-bulk modulus model, the bulk modulus-shear modulus model proposed by Domaschu et al.[13], etc. However, the nonlinear elastic model has limitations in describing the strain softening and dilatancy characteristics of soil, and it cannot adapt well to different stress paths. On the other hand, a large number of data show that in K_0 consolidation or constant stress ratio stress path tests, the deformation of granular soil is mainly attributed to bulk compression, while strain softening and dilatancy properties are not obvious[6−7, 14−15], which is quite different from other triaxial stress path tests. For example, Bian et al.[16] found that in different stress path tests of rockfill materials the dilatancy equation of the generalized plasticity model under the conventional triaxial test was not applicable to the constant stress ratio path test. Therefore, as a simple and practical earthfill calculation model, there are still obvious practical advantages in using the nonlinear elastic model to describe the stress–strain relationship under the earthfill stress path.

Unlike the linear elastic model, the stress–strain relationship of the nonlinear elastic model cannot be expressed by physical constants, but is described by functional parameters of deformation. The selection of these functions often depends on the specific stress path test[17]. The Duncan-Chang model[11] is a commonly used nonlinear elastic model. Its proposal is attributed to the hyperbolic relationship developed by Kondner[18] based on a large number of triaxial stress–strain curves of soil. Since the model parameters are easy to be determined by conventional triaxial tests, the nonlinear elastic model is widely used in soil stress–deformation analysis[19−20]. However, the stress–strain relationship of the earthfill stress path is different from the hyperbolic relationship of other triaxial stress path tests. The calculation error is large when the hyperbolic nonlinear elastic model is used. Therefore, it is necessary to simulate the actual situation of the earthfill stress path through tests to obtain the stress–strain relationship and deformation parameters that can reflect the influence of the earthfill stress path. In addition, coral sand particles can be broken under the normal stress. Therefore, it is necessary to understand the particle breakage status under the earthfill stress path to assess the potential impact of particle breakage on the deformation properties of coral sand.

In light of the above, based on the generalized Hooke's law, a nonlinear elastic model in the form of a power function is first proposed to describe the stress–strain curve of coral sand, and the expression of deformation parameters are given. Meanwhile, a series of K_0 consolidation tests and triaxial compression tests with the constant stress ratio path is conducted on coral sand to investigate the stress–strain relation- ship and the behavior of particle breakage. The applicability of the power-law stress–strain model for coral sand is investigated. Finally, the calculated results of the model are compared with the test curves to examine the prediction effect of the power-law model on deformation. The results are expected to provide references for the design and construction of islands and reefs.

2 Power-law stress–strain model

2.1 Power-function stress-strain relationship

The stress in this paper is uniformly expressed as the effective stress, and the symbolic meanings of stress and strain under axisymmetric conditions are predefined as follows: σ_1' is the axial effective stress; σ_3' is the effective confining pressure; $q=\sigma_1'-\sigma_3'$ is the deviatoric stress; $p'=(\sigma_1'+2\sigma_3')/3$ is the average effective principle stress; $K=\mathrm{d}\sigma_3'/\mathrm{d}\sigma_1'$ is the principle stress increment ratio; ε_1 is the axial strain; ε_3 is the radial strain; ε_v is the volumetric strain; and $\varepsilon_s=\varepsilon_1-\varepsilon_v/3$ is the shear strain.

The power-law stress–strain curve of soil can usually be expressed as

$$\frac{\sigma_1'}{p_a}=A\varepsilon_1^B \tag{1}$$

where A and B are both test constants; p_a = 101.33 kPa is the standard atmospheric pressure. The introduction of p_a is to make test constants dimensionless quantities to adapt to different measurement units.

A large number of tests show that the stress–strain curves of granular soils such as quartz sand and rockfill materials under the constant stress ratio path can be described by the power-function stress–strain relationship of Eq. (1)[6−7, 21]. Since the theoretical basis of the nonlinear elastic model is still elastic theory, the stress–strain relationship can be expressed by increments of stress and strain, and is related by the tangent modulus and tangent Poisson's ratio.

2.2 Tangent Poisson's ratio

According to the generalized Hooke's law, the axial strain and radial strain under axisymmetric conditions are

$$\varepsilon_1=\frac{1}{E}(\sigma_1'-2\mu\sigma_3') \tag{2}$$

$$\varepsilon_3=\frac{1}{E}\left[\sigma_3'-\mu(\sigma_1'+\sigma_3')\right] \tag{3}$$

Dividing Eq. (3) by Eq. (2) yields

$$\frac{\varepsilon_3}{\varepsilon_1}=\frac{\sigma_3'-\mu(\sigma_1'+\sigma_3')}{\sigma_1'-2\mu\sigma_3'} \tag{4}$$

Rewrite the stress and strain in Eq. (4) in the form of the increment, and then substitute $K=\mathrm{d}\sigma_3'/\mathrm{d}\sigma_1'$ under the constant stress ratio path into Eq. (4). The tangent Poisson's ratio can be obtained:

$$\mu_t = \frac{K - \mathrm{d}\varepsilon_3/\mathrm{d}\varepsilon_1}{1 + K - 2K(\mathrm{d}\varepsilon_3/\mathrm{d}\varepsilon_1)} \tag{5}$$

Based on the volumetric strain $\varepsilon_v = \varepsilon_1 + 2\varepsilon_3$ under the axisymmetric condition, then $\varepsilon_3 = (\varepsilon_v - \varepsilon_1)/2$ is obtained. It can be rewritten in the form of the increment:

$$\frac{\mathrm{d}\varepsilon_3}{\mathrm{d}\varepsilon_1} = \frac{1}{2}\left(\frac{\mathrm{d}\varepsilon_v}{\mathrm{d}\varepsilon_1} - 1\right) \tag{6}$$

Substituting Eq. (6) into Eq. (5) yields

$$\mu_t = \frac{1 + 2K - \mathrm{d}\varepsilon_v/\mathrm{d}\varepsilon_1}{2\left[1 + 2K - K(\mathrm{d}\varepsilon_v/\mathrm{d}\varepsilon_1)\right]} \tag{7}$$

Eq. (7) shows that the tangent Poisson's ratio is related to the ratio $\mathrm{d}\varepsilon_v/\mathrm{d}\varepsilon_1$ of the volumetric strain increment and the axial strain increment, and the stress ratio *K*.

Under K_0 condition, $\mathrm{d}\varepsilon_3 = 0$. According to Eq. (6), $\mathrm{d}\varepsilon_v / \mathrm{d}\varepsilon_1 = 1$. Substituting it into Eq. (7), it can be seen that the tangent Poisson's ratio under K_0 condition is consistent with the results of literature [15].

2.3 Tangent modulus

By rewriting Eq. (2) in the form of the stress increment and strain increment and substituting it into Eq. $\mathrm{d}\sigma_3'/\mathrm{d}\sigma_1' = K$, the following equation can be obtained

$$\mathrm{d}\varepsilon_1 = \frac{1 - 2\mu_t K}{E_t}\mathrm{d}\sigma_1' \tag{8}$$

where E_t is the tangent elastic modulus.

Substituting the stress–strain relationship of Eq. (1) into Eq. (8), the tangent elastic modulus can be expressed by the axial strain as follows:

$$\frac{E_t}{p_a} = AB\varepsilon_1^{B-1}\left(1 - 2\mu_t K\right) \tag{9}$$

Rewriting Eq. (1) yields $\varepsilon_1 = (1/A)^{1/B} \times (\sigma_1'/p_a)^{1/B}$. By substituting it and Eq. (7) into Eq. (9), the tangent elastic modulus can be expressed by the axial effective stress:

$$\frac{E_t}{p_a} = BA^{\frac{1}{B}}\left(\frac{\sigma_1'}{p_a}\right)^{\frac{B-1}{B}} \cdot \frac{1 + K - 2K^2}{1 + 2K - K \cdot \mathrm{d}\varepsilon_v/\mathrm{d}\varepsilon_1} \tag{10}$$

In the nonlinear elastic model, the relationship between the deviatoric stress $\mathrm{d}q$ and shear strain $\mathrm{d}\varepsilon_s$, the average effective principal stress $\mathrm{d}p'$ and volumetric strain $\mathrm{d}\varepsilon_v$ characterized in increments, can be related by the tangent shear modulus G_t and tangent volumetric modulus K_t, respectively. That is,

$$\mathrm{d}\varepsilon_s = \frac{1}{3G_t}\mathrm{d}q \tag{11}$$

$$\mathrm{d}\varepsilon_v = \frac{1}{K_t}\mathrm{d}p' \tag{12}$$

According to the generalized Hooke's law, in the nonlinear elastic model, G_t and K_t can be obtained from E_t and μ_t. That is,

$$G_t = \frac{E_t}{2(1 + \mu_t)} \tag{13}$$

$$K_t = \frac{E_t}{3(1 - 2\mu_t)} \tag{14}$$

By substituting Eqs. (13) and (14) into the Eq. (10), tangent moduli G_t and K_t of the power-law stress-strain model can be obtained:

$$\frac{G_t}{p_a} = BA^{\frac{1}{B}}\left(\frac{\sigma_1'}{p_a}\right)^{\frac{B-1}{B}} \cdot \frac{1 - K}{3 - \mathrm{d}\varepsilon_v/\mathrm{d}\varepsilon_1} \tag{15}$$

$$\frac{K_t}{p_a} = BA^{\frac{1}{B}}\left(\frac{\sigma_1'}{p_a}\right)^{\frac{B-1}{B}} \cdot \frac{1 + 2K}{3 \times \mathrm{d}\varepsilon_v/\mathrm{d}\varepsilon_1} \tag{16}$$

By substituting $\mathrm{d}\varepsilon_v/\mathrm{d}\varepsilon_1 = 1$ under the K_0 condition into Eqs. (10), (15) and (16), it can been seen that the tangent modulus is related to K_0, which is consistent with literature [15].

According to Eqs. (7), (10), (15) and (16), the tangent Poisson's ratio μ_t and the three tangent moduli E_t, G_t and K_t of the power-function nonlinear elastic model can be expressed as functions of the axial effective stress. In addition to test constants *A* and *B*, they can also be described by the ratio $\mathrm{d}\varepsilon_v / \mathrm{d}\varepsilon_1$ and stress ratio *K*.

3 Materials and methods

3.1 Test soil sample

The test soil samples were taken from the coral sand of an island reef in the South China Sea. Based on the test results[22], the equivalent $CaCO_3$ content of the coral sand was 96.39%. The specific gravity of soil particles was $G_s = 2.75$. The maximum void ratio was $e_{max} = 1.32$, and the minimum void ratio was $e_{min} = 0.75$. The average particle diameter was $d_{50} = 0.6$ mm. The uniformity coefficient was $C_u = 2.8$. The particle size distribution curve is shown in Fig. 1.

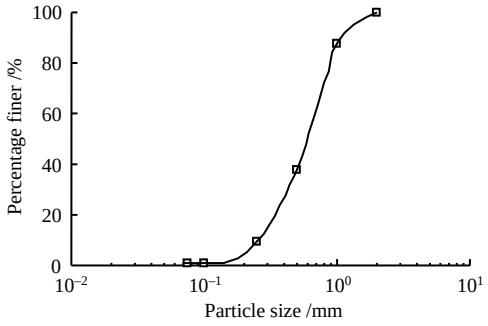

Fig. 1 Particle-size distribution curve of coral sand

3.2 Test apparatus

As shown in Fig. 2, the fully automatic triaxial test system produced by British GDS Company is adopted as the test apparatus. It is mainly composed of a

triaxial pressure chamber, three digital pressure/volume controllers (DPVC1-3), a data logger, a computer, etc. Among them, DPVC1 controls the axial load; DPVC2 controls the back pressure (or pore pressure) and measures the volumetric strain of the sample; DPVC3 controls the confining pressure and the pore pressure is measured by the sensor at the bottom of the pressure chamber. The data logger is responsible for storing the test data collected by the sensor.

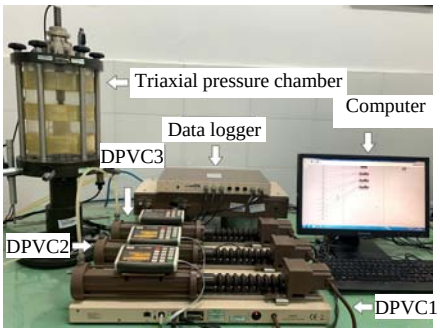

Fig. 2 Test apparatus

3.3 Sample preparation and saturation

The sample is cylindrical, with a diameter of 39.1 mm and a height of 80 mm. In order to accurately control the initial relative density of the sample, the sample was prepared by the sand pluviation method through pouring dry sand, as shown in Fig.3. The rubber membrane was wrapped on the cylindrical base of the triaxial apparatus, and the required mass of dried sand sample is weighed. The correlation between the height of sand falling and the sample density was determined by the test. Then, the sand funnel was used to sprinkle dry sand in the membrane in three equal layers to prepare a sample with a relative density of $D_r = 75\ \%$.

Fig. 3 Sample preparation with sand pluviation method

The methods of water head saturation and back pressure saturation were used for sample saturation. Firstly, 5–10 kPa CO_2 gas was introduced from the bottom of the sample to replace the air in the pores of the sample. Then, the drainage pipe was used to circulate the airless water from the bottom of the sample. Finally, the back pressure saturation was applied by the triaxial test system. The steps of applying back pressure were as follows: first, a confining pressure of 20 kPa was applied to the sample for preloading, and then the back pressure was applied step by step with 50 kPa per stage. To reduce the disturbance to the sample, the confining pressure should be applied synchronously when the back pressure was applied, and the confining pressure should always be 20 kPa larger than the back pressure. The pore pressure coefficient B was measured for each level of back pressure. When $B > 0.95$ was detected, the sample was considered to be completely saturated.

3.4 Test methods

K_0 test was stress-controlled, and the confining pressure and axial pressure were applied simultaneously during the test. The loading rate of the confining pressure was 5 kPa/min. The volume change of the sample was adjusted according to the axial strain through DPVC of the triaxial test system to keep the changes of the volumetric strain and axial strain of the sample equal ($\mathrm{d}\varepsilon_v / \mathrm{d}\varepsilon_1 = 1$), and the radial strain change was 0 ($\mathrm{d}\varepsilon_3 = 0$). The test was terminated when loaded to 450 kPa, and the coefficient of earth pressure at rest was calculated through $K_0 = \sigma_3'/\sigma_1'$.

The drained triaxial compression test under the constant stress ratio path was stress-controlled, and a total of 8 constant stress ratio tests with different stress ratios K were carried out. During the tests, K was set to be 0.25, 0.30, 0.35, 0.40, 0.45, 0.50, 0.55 and 0.60, respectively, and then the axial stress and confining pressure were increased simultaneously according to the set K. The axial loading rate was $\mathrm{d}\sigma_1' = 5$ kPa/min, and the test was terminated when σ_1' was close to 1 450 kPa. It should be pointed out that the stress of coral sand in the drained triaxial test is the effective stress. The effective stress paths of each test in q- p' plane are shown in Fig.4.

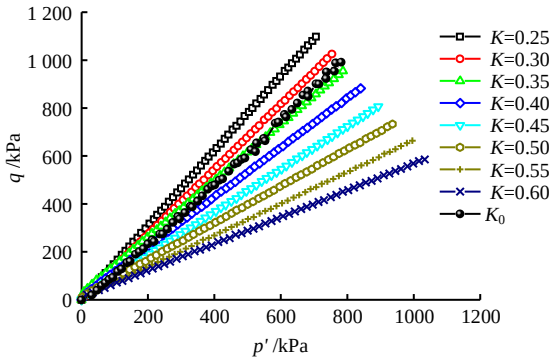

Fig. 4 Stress path in q– p' plane

After the test, for each sample, the particle size distribution curve was obtained by the sieve analysis method, and the relative breakage index B_r of Hardin[23] was used to quantify the particle breakage of coral sand, as shown in Fig. 5. The areas enclosed by the particle size distribution curves before and after the test and the 0.075 mm particle size cutoff line are defined as the pre-test breakage potential A_{abda} and the post-test breakage potential A_{acda}. The difference A_{abca} between the two is defined as the amount of

breakage. Then, B_r is the ratio of the amount of breakage to the pre-test breakage potential ($B_r = A_{abca} / A_{abda}$).

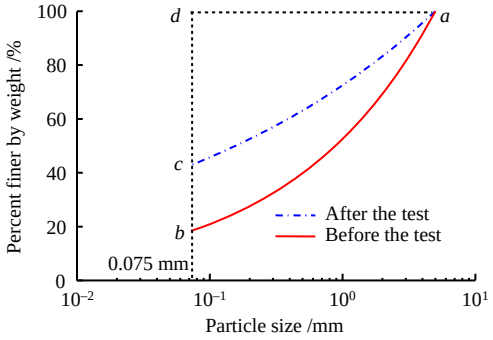

Fig. 5 Definition of Hardin's relative breakage index

4 Results and analysis

4.1 Coefficient of earth pressure at rest

Figure 6 shows the variation of the coefficient of earth pressure at rest with the axial effective stress. It can be seen that at the beginning of K_0 test, the K_0 - σ_1' curve drops sharply and then gradually becomes gentle. Many scholars have observed similar phenomena in K_0 tests conducted in the triaxial apparatus[15, 24-25]. It can be explained as follows: the sample is saturated by the back pressure of the triaxial apparatus, so that K_0 test does not start from the zero stress state, but there is an initial isotropic consolidation stress of $\sigma_3' = 20$ kPa. That is, K_0 test is loaded from the isotropic state. Thus, the initial K_0 value is 1. With the simultaneous application of the axial effective stress and effective confining pressure, the sample gradually transits to the K_0 stress state, and K_0 rapidly decreases from the initial value to the actual value. Therefore, there is a transition process from the isotropic stress state to K_0 stress state.

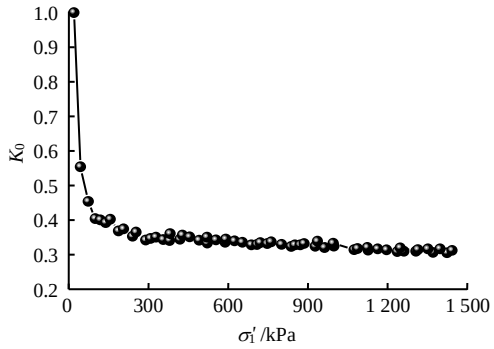

Fig. 6 Curve of K_0 versus axial effective stress

Figure 6 also shows that the coefficient of earth pressure at rest of coral sand is not a constant, but decreases slowly with the continuous increase of the axial effective stress. It indicates that K_0 value is affected by the stress state. Many scholars have obtained the same conclusion[24-25]. For the coral sand in this study, the actual K_0 value varies between 0.31 and 0.40.

4.2 Stress–strain curve

Figure 7 shows the relationship between the axial effective stress σ_1' and axial strain ε_1 of different K values in the constant stress ratio test and K_0 test. It can be found that the $\sigma_1' - \varepsilon_1$ curve of the constant stress ratio test is affected by K. As K value increases, the axial effective stress at the same axial strain also increases, and $\sigma_1' - \varepsilon_1$ curve gradually becomes steeper. The variation pattern of $\sigma_1' - \varepsilon_1$ curve of K_0 test is similar to that of the constant stress ratio test. It is located between the curves of K = 0.35 and K = 0.40. It is consistent with the variation range of K_0 values from 0.31 to 0.40.

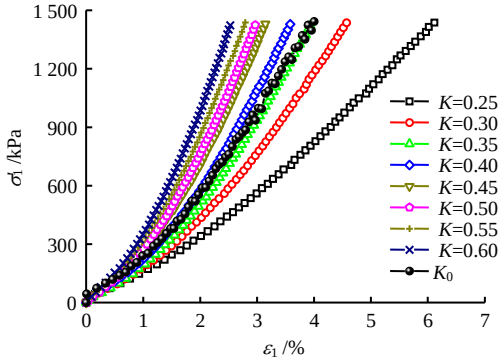

Fig. 7 Curves of axial effective stress versus axial strain

To verify the applicability of the power-law stress–strain model to coral sand, the regression analysis of $\sigma_1' - \varepsilon_1$ relationships of the constant stress ratio test and K_0 test is performed according to Eq. (1). The regression values of the test constants and the coefficient of determination R^2 are shown in Table 1. It can been seen that all R^2 values are larger than 0.994, indicating that the significance of the regression analysis is high. Therefore, $\sigma_1' - \varepsilon_1$ curves of the constant stress ratio test and K_0 test can be described by the power-law model.

The average effective principal stress p', deviatoric stress q, and axial stress σ_1' of the constant stress ratio (or K_0) test can be converted through K (or K_0). That is, $q = (1-K)\sigma_1'$ and $p' = (1+2K)\sigma_1'/3$. Therefore, q-ε_s and p'-ε_v curves can also be described by the power-law stress–strain model.

Table 1 Test regression values of parameters and coefficient of determination for Eqs. (1) and (17)

Stress increment ratio K	Eq. (1)			Eq. (17)		
	A	B	R^2	C	D	R^2
0.25	437.5	1.36	0.997 5	0.78	0.37	0.964 9
0.30	922.6	1.37	0.996 8	0.99	0.36	0.935 6
0.35	1 438.8	1.41	0.997 5	1.15	0.34	0.929 5
0.40	1 386.8	1.39	0.994 8	1.40	0.35	0.912 1
0.45	1 671.1	1.39	0.996 1	1.48	0.37	0.940 5
0.50	2 147.8	1.41	0.996 8	1.56	0.36	0.915 2
0.55	2 013.7	1.40	0.996 3	1.69	0.37	0.917 3
0.60	2 187.8	1.39	0.994 8	1.88	0.39	0.918 6
K_0	893.3	1.29	0.996 3	1.00	0.00	1.000 0

Figure 8 illustrates the relationship between volumetric strain and axial strain under the constant stress ratio test and K_0 test. It can be found that $\varepsilon_v-\varepsilon_1$ curve is a straight line due to $\mathrm{d}\varepsilon_v/\mathrm{d}\varepsilon_1=1$ in K_0 test. The $\varepsilon_v-\varepsilon_1$ curve of the constant stress ratio test gradually becomes gentle with the increase of the axial strain, showing obvious nonlinear characteristics. It indicates that the tangent slope $\mathrm{d}\varepsilon_v/\mathrm{d}\varepsilon_1$ of $\varepsilon_v-\varepsilon_1$ curve is not a constant, but varies with the change of axial strain. In addition, $\varepsilon_v-\varepsilon_1$ curve is also affected by K value, and gradually becomes flat with the decrease of K. The reason is that from the effective stress path of Fig. 4, the smaller the K value, the greater the weight of the deviatoric stress q. Therefore, the coral sand is relatively easy to enter the plastic state.

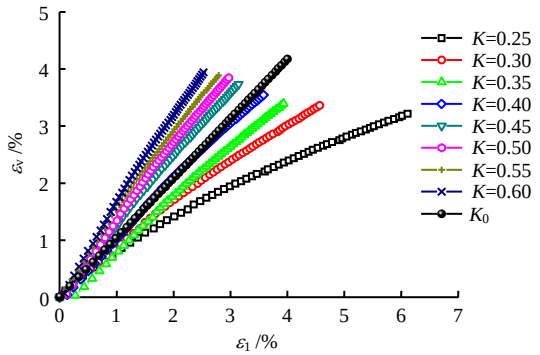

Fig. 8 Curves of volumetric strain versus axial strain

Figure 9 shows the relationship between the ratio of the volumetric strain increment to the axial strain increment and axial effective stress in the constant stress ratio test and K_0 test. Fig. 9(a) presents the variation of $\mathrm{d}\varepsilon_v/\mathrm{d}\varepsilon_1$ with stress σ_1'. As shown in the figure, as σ_1' increases, $\mathrm{d}\varepsilon_v/\mathrm{d}\varepsilon_1$ first decreases sharply and then becomes gentle. The relationship between $\mathrm{d}\varepsilon_v/\mathrm{d}\varepsilon_1$ and the logarithm $\lg(\sigma_1'/p_a)$ of the axial effective stress is plotted in Fig.9 (b). It shows an approximate linear relationship between $\mathrm{d}\varepsilon_v/\mathrm{d}\varepsilon_1$ and $\lg(\sigma_1'/p_a)$:

$$\frac{\mathrm{d}\varepsilon_v}{\mathrm{d}\varepsilon_1}=C-D\lg\frac{\sigma_1'}{p_a} \tag{17}$$

where C and D are test constants.

According to Eq. (17), the linear regression analysis of $\mathrm{d}\varepsilon_v/\mathrm{d}\varepsilon_1-\lg(\sigma_1'/p_a)$ relationship is performed. The regression values of test constants C and D and coefficient of determination are shown in Table 1. One can see that R^2 values are all greater than 0.91, indicating a high significance of the linear regression analysis.

It should be pointed out that although $\sigma_1'-\varepsilon_1$ curves of the constant stress ratio with different K values and K_0 test can be expressed as power-law relationships, the two are not exactly the same. As shown in Fig. 9, $\mathrm{d}\varepsilon_v/\mathrm{d}\varepsilon_1$ of the constant stress ratio test decreases with the increase of σ_1'. However, in K_0 test, to maintain K_0 conditions of $\mathrm{d}\varepsilon_v/\mathrm{d}\varepsilon_1=1$ and $\mathrm{d}\varepsilon_3=0$, the effective principal stress ratio K_0 is not a constant, but decreases slowly with the test proceeding, as shown in Fig.6. Therefore, it is actually a stress path test with variable stress ratios.

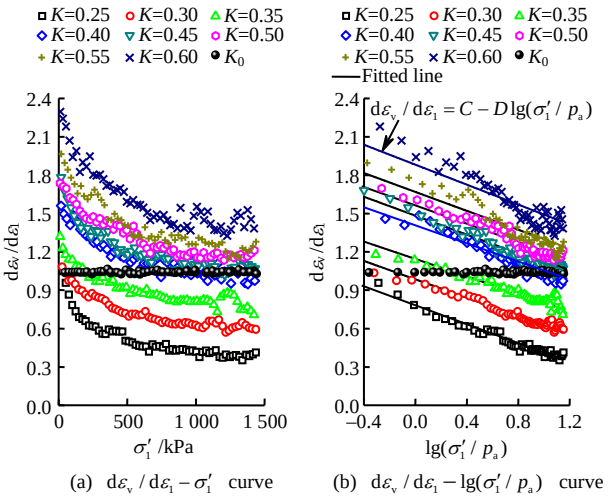

(a) $\mathrm{d}\varepsilon_v/\mathrm{d}\varepsilon_1-\sigma_1'$ curve (b) $\mathrm{d}\varepsilon_v/\mathrm{d}\varepsilon_1-\lg(\sigma_1'/p_a)$ curve

Fig. 9 Curves of dεv/dε1 versus axial effective stress

4.3 Deformation parameters

The variation of deformation parameters with stress can be obtained by substituting the test results in this study into the expression of deformation parameters. The test regression values of C and D in Table 1 are substituted into Eq. (17) to determine $\mathrm{d}\varepsilon_v/\mathrm{d}\varepsilon_1$. Then, the relationship between the tangent Poisson's ratio μ_t and σ_1' can be obtained by substituting $\mathrm{d}\varepsilon_v/\mathrm{d}\varepsilon_1$ and K (or K_0) values into Eq. (7), as shown in Fig. 10. It can be found that the tangent Poisson's ratios are not constant. In the constant stress ratio test, μ_t gradually increases with the increase of σ_1'. Under the same σ_1' condition, a larger K results in a smaller μ_t. In K_0 test, μ_t gradually decreases with the increase of σ_1'. Under the test conditions in this study, the actual range of the tangent Poisson's ratio of coral sand is 0.15–0.40 in the constant stress ratio test and 0.23–0.28 in K_0 test.

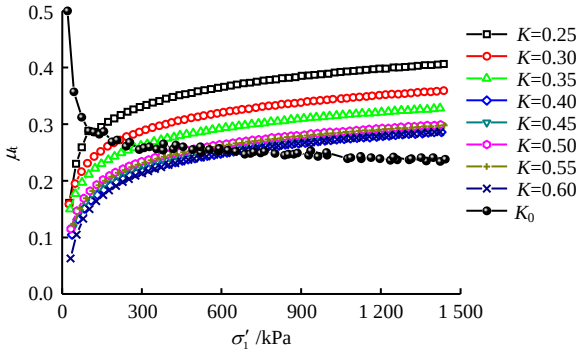

Fig. 10 Curves of tangent Poisson's ratio versus axial effective stress

The method for determining the tangent moduli is as follows: $\mathrm{d}\varepsilon_v/\mathrm{d}\varepsilon_1$ determined by the test, the regression values of A, B and K or measured K_0 in Table 1 are substituted into the Eqs. (10), (15) and

(16), and then the variation of the tangent moduli E_t, G_t and K_t with σ_1' can be obtained, as shown in Fig. 11. It shows that the tangent moduli E_t, G_t and K_t increase gradually with the increase of σ_1'. Under the same σ_1' condition, a larger K (or K_0) leads to larger E_t and G_t while E_t curves are intertwined and overlapped. Comparing K_0 test with the constant stress ratio test with a similar K value, the relationship between E_t and σ_1' is basically the same as that between G_t and σ_1', while quite different from relationship between K_t and σ_1'. Under the test conditions in this study, the ranges of the deformation moduli of coral sand are as follows: for the constant stress ratio test, E_t, G_t and K_t range from 7.6 to 49.1 MPa, from 3.2 to 19.1 MPa, and from 6.7 to 39.9 MPa, respectively; for K_0 test, E_t, G_t and K_t range from 12.7 to 39.2 MPa, from 4.7 to 15.8 MPa, and from 14.7 to 24.9 MPa, respectively.

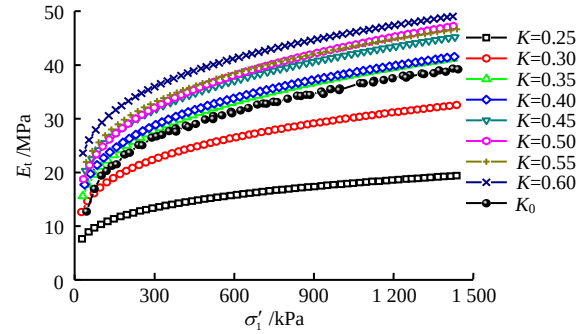

(a) E_t- σ_1' curve

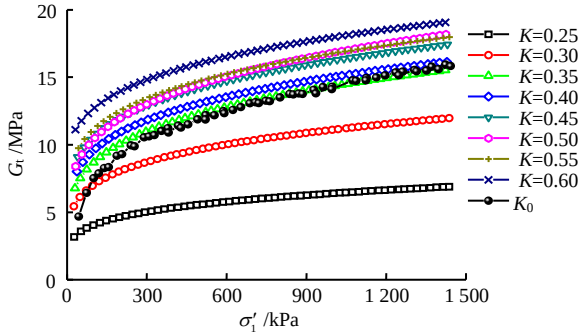

(b) G_t- σ_1' curve

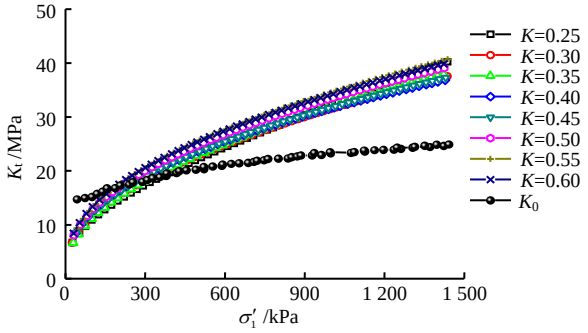

(c) K_t- σ_1' curve

Fig. 11 Curves of tangent modulus versus axial effective stress

4.4 Relative breakage index

Figure 12 shows the relationships between the relative breakage index B_r and K measured at the end of each test, and between the corresponding average effective principal stress p'_{max} and deviatoric stress q_{max}. It can be found that B_r increases as K increases (see Fig. 12(a)). The corresponding proportion of p'_{max} increases and the proportion of q_{max} decreases (see Fig. 12(b)). It indicates that with the increase of K, the sample mainly exhibits volumetric compression properties. At the end of K_0 test, K_0 = 0.31. Compared with the constant stress ratio test with similar K value (0.30–0.35), the effective stress of the sample is basically the same, as shown in Fig. 12(b). However, B_r increases significantly, as shown in Fig. 12(a). It may be related to the larger volumetric strain of K_0 test under the same axial effective stress condition, as shown in Fig. 8. Within the test stress range of this study, the relative breakage index of coral sand at the end of each test is very small. B_r ranges from 0.20% to 0.45%. It suggests that particle breakage has little effect on K_0 consolidation and the constant stress ratio test.

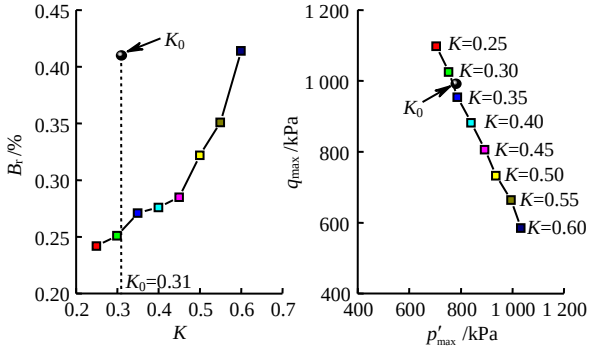

(a) B_r–K (b) q_{max}– p'_{max} 系

Fig. 12 Relationships between B_r, q_{max}, p'_{max} and stress ratio

5 Comparison between model calculation and test curves

5.1 Determination of model parameters

As mentioned above, the power-law stress–strain model established in this study contains test constants A, B, C, D and stress ratio K (or K_0) and other parameters. An example of the constant stress ratio test is presented as follows to illustrate the model calculation method and the rationality of its prediction on deformation by comparing the curves of model calculation and the test.

The variations of test constants A, B, C and D with stress ratio K in Table 1 are investigated to establish the correlation between them. The analysis shows that A and C increase with the increase of K, where A and K satisfy the quadratic function relationship. The regression analysis results are shown in Fig.13(a). There is a linear relationship between C and K, and the linear regression results are shown in Fig. 13(b). B and D vary little as K increase, where D is the slope of the linear relationship of $d\varepsilon_v / d\varepsilon_1 - \lg(\sigma_1' / p_a)$. It can

be seen from Fig. 9(b) that the fitted lines of different K values remain roughly parallel. Thus, B and D can be approximated as constants. The calculation formula of regression values of test constants A, B, C and D and related parameters are shown in Table 2. It indicates that the calculated regression values of A, B, C and D can be expressed by six parameters a_1, b_1, c_1, d_1, a_2 and b_2.

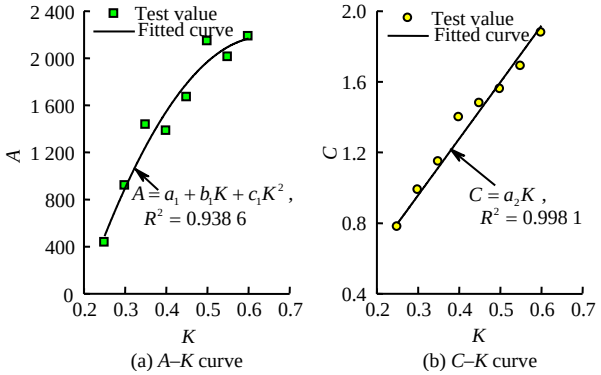

(a) A–K curve (b) C–K curve

Fig. 13 Fitted curves of A, C versus K

Table 2 Regression formulas and parameter values

Test parameters	Regression formulas	Reference values
A	$A = a_1 + b_1K + c_1K^2$	$a_1 = -2\,400$, $b_1 = 14\,375$, $c_1 = -11\,276$
B	$B = d_1$	$d_1 = 1.41$
C	$C = a_2K$	$a_2 = 3.20$
D	$D = b_2$	$b_2 = 0.36$

Table 2 shows that the power-law stress–strain model expresses the tangent Poisson's ratio μ_t and three tangent moduli E_t, G_t and K_t, through six parameters. As a results, it succeeds in describing the stress–strain curve under the constant stress ratio path within a certain range of K values.

5.2 Comparison of stress-stain curves

The model calculation results in this study are compared with the test curves to verify the applicability of the power-law stress–strain model and deformation parameters under the constant stress ratio path within a certain range of K values. The computational procedure is as follows:

(1) The stress ratio K of the constant stress ratio test is substituted into the regression value calculation formula in Table 2. Then, the calculated regression values of test constants A, B, C and D are obtained. The results are shown in Table 3.

(2) Substitute the calculated regression values of C and D into Eq. (17) to determine ratio $\mathrm{d}\varepsilon_v / \mathrm{d}\varepsilon_1$, and then substitute it and calculated regression values of A and B into Eqs. (7), (10), (15) and (16) to determine μ_t, E_t, G_t and K_t.

(3) Give smaller stress increment steps $\mathrm{d}\sigma_1'$, $\mathrm{d}q$ and $\mathrm{d}p'$ first. Then, by substituting the calculated μ_t, E_t, G_t and K_t into the Eqs. (8), (11), (12), respectively, the corresponding strain increment values $\mathrm{d}\varepsilon_1$, $\mathrm{d}\varepsilon_s$ and $\mathrm{d}\varepsilon_v$ can be obtained. Finally, the stress increments and strain increments are accumulated, and the full expressions of $\sigma_1' - \varepsilon_1$, $q - \varepsilon_s$, $p' - \varepsilon_v$ and $\varepsilon_v - \varepsilon_1$ curves can be obtained.

The $\sigma_1' - \varepsilon_1$ and $q - \varepsilon_s$ curves calculated by the model are compared with the test curves to verify the prediction effect of the axial strain and shear strain under different K values. In the constant stress ratio test with different K values, $p' - \varepsilon_v$ curves overlap each other. Thus, it is difficult to compare them in the same figure. However, the prediction effect of volumetric strain of different K values can be verified by comparing the $\varepsilon_v - \varepsilon_1$ curves. The comparison between the predicted results and test results of these stress–strain curves is shown in Fig. 14.

Table 3 Calculated regression values of test parameters

Stress ratio	Test parameters			
K	A	B	C	D
0.25	489.0	1.41	0.80	0.36
0.30	897.7	1.41	0.96	0.36
0.35	1 249.9	1.41	1.12	0.36
0.40	1 545.8	1.41	1.28	0.36
0.45	1 785.4	1.41	1.44	0.36
0.50	1 968.5	1.41	1.60	0.36
0.55	2 095.3	1.41	1.76	0.36
0.60	2 165.6	1.41	1.92	0.36

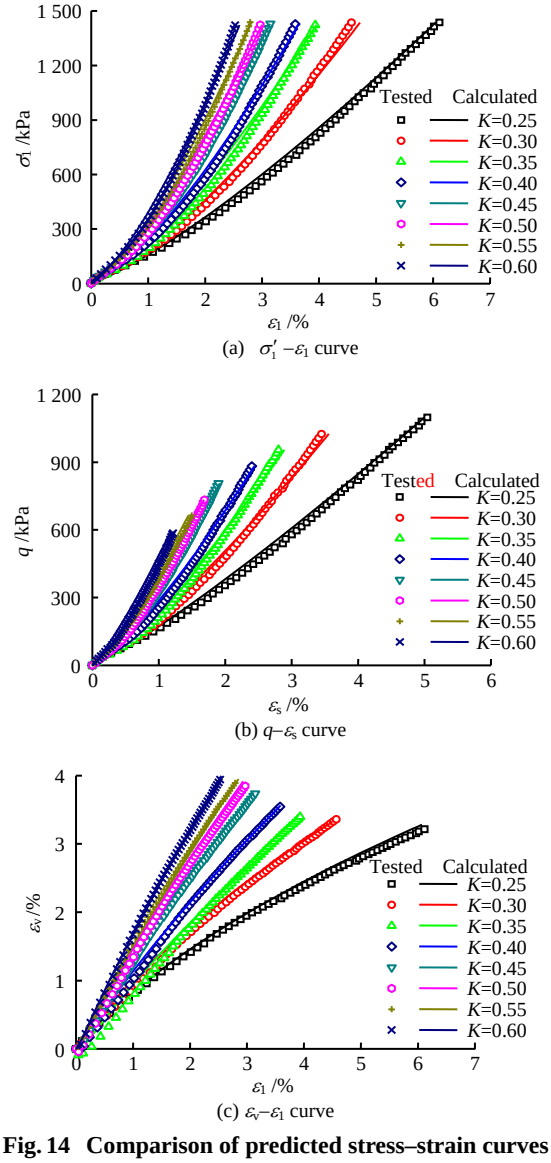

(a) $\sigma_1' - \varepsilon_1$ curve

(b) $q - \varepsilon_s$ curve

(c) $\varepsilon_v - \varepsilon_1$ curve

Fig. 14 Comparison of predicted stress–strain curves with experimental results

It can be observed from Fig. 14 that the prediction results of the power-law model for each stress–strain curve are in good agreement with test curves, and the maximum errors between them are about 3.0% in axial strain, 3.8% in shear strain, and 2.2% in volumetric strain. It suggests that the power-law model can reasonably predict the axial strain, shear strain and volumetric strain of coral sand under the constant stress ratio path within a certain range of K values and stress. Therefore, the deformation of coral sand during the filling period can be calculated and analyzed by combining with the finite element program. The power-law model and deformation parameters not only reflect the influence of the constant stress ratio path with different K values on the stress–strain relationship, but also are clear in concept, simple and practical, and convenient for engineering calculation and analysis.

Notably, although the power-law stress–strain model established in this paper is still a fitted model based on test data, it is still very difficult to establish a stress-strain model suitable for various properties, initial states, and stress paths of coral sands, considering that the engineering properties of coral sands are complex and their stress-strain relationships are affected by many factors. Therefore, before this problem is solved perfectly, a reasonable and feasible method is to establish a concise and practical nonlinear elastic model first. Then, for the coral sand with selected relative density and gradation, the relevant test constants and geotechnical parameters can be measured by the triaxial test simulating the actual earthfill stress path, so as to determine the relationship between deformation parameters and stress or strain. Finally, the obtained calculation model is combined with the finite element program to analyze and predict the settlement of the actual project. Therefore, the fitted model based on the test data is still important and applicable in engineering practice.

6 Conclusions

In this study, a power-law nonlinear elastic model describing the stress–strain relationship of soil during the filling period is established, and a series of triaxial tests on coral sand under K_0 consolidation and constant stress ratio paths is carried out. Finally, the applicability of the power-law stress–strain model is investigated. The main conclusions can be drawn as follows:

(1) The stress–strain curves of coral sand under K_0 consolidation and constant stress ratio path have the characteristics of power-function curves. A power-law nonlinear elastic model is established to describe the stress–strain relationship. The deformation parameters of the model can be expressed as functions of the axial effective stress.

(2) In the power-law model, the tangent moduli and tangent Poisson's ratio are expressed through the parameters related to the stress ratio K. It succeeds in describing the stress–strain curve under the constant stress ratio path.

(3) Within the stress range of the test in this study, whether in K_0 consolidation or constant stress ratio tests, the particle breakage amount of coral sand is very small, and it has little effect on the stress–strain characteristics.

(4) The tangent Poisson's ratio and tangent moduli under the constant stress ratio path increase with the increase of the axial effective stress. Under the same axial effective stress condition, the greater the stress ratio K value, the greater the tangent moduli, and the smaller the tangent Poisson's ratio. With the increase of the axial effective stress, under K_0 consolidation, the coefficient K_0 and tangent Poisson's ratio of coral sand decrease, and the tangent moduli increase.

(5) The power-law model reasonably predicts the stress–strain relationship of coral sand under constant stress ratio paths within a certain range of stress ratio K and stress. The model and model parameters reflect the influence of the stress path of the constant stress ratio on the stress–strain relationship. Furthermore, the model is simple and convenient for engineering practice, and the parameters are easy to be obtained.

References

[1] QIN Zhi-guang, YUAN Xiao-ming, CAO Zhen-zhong, et al. Applicability and quality evaluation of foundation treatment method for backfilled coral sand site[J]. Journal of Natural Disasters, 2021, 30(1): 78–88.

[2] WEN Bing, YUAN Nei-zhen, KONG Ling-wei, et al. Application practice and settlement estimation of composite ground for high-rise buildings on coral sand site of hydraulic fill[J]. China Civil Engineering Journal, 2021, 54(12): 85–93.

[3] QIU Wei-jian, YANG He-ping, HE Ying-xi, et al. Experimental study on coral reef sand as hydraulic filling materials for foundation and its vibroflotation compaction[J]. Chinese Journal of Geotechnical Engineering, 2017, 39(8): 1517–1523.

[4] ZHANG Lei, XIAO Guo-hua, ZHANG Jin-xun, et al. Study on foundation treatment of airport runway with dredged coral sand[J]. Construction Technology, 2019, 48(4): 40–43.

[5] WANG Xin-zhi, CHEN Min, WEI Hou-zhen, et al. Experimental study on dynamic response of calcareous sand subgrade under vehicle load[J]. Rock and Soil Mechanics, 2018, 39(11): 4093–4101.

[6] LIU Zu-de, LU Shi-qiang, YANG Tian-lin, et al. The influence of stress path on the stress-strain behavior of earthfills its application[J]. Chinese Journal of Geotechnical Engineering, 1982, 4(4): 45–55.

[7] SUN Yue-song, PU Jia-liu, LI Guang-xin. The effects of different stress paths on stress-strain behavior of sand[J].

Chinese Journal of Geotechnical Engineering, 1987, 9(6): 78–88.

[8] ROSCOE K H, SCHOFIELD A N, WROTH C P. On the yielding of soils[J]. Géotechnique, 1958, 8(1): 22–53.

[9] ROSCOE K H, SCHOFIELD A N, THURAIRAJAH A. Yielding of clays in states wetter than critical[J]. Géotechnique, 1963, 13(3): 211–240.

[10] LADE P V, DUNCAN J M. Elastoplastic stress-strain theory for cohesionless soil[J]. Journal of the Geotechnical Engineering Division, ASCE, 1975, 101(10): 1037–1053.

[11] DUNCAN J M, CHANG C Y. Nonlinear analysis of stress and strain in soils[J]. Journal of the Soil Mechanics and Foundation Division, ASCE, 1970, 96(SM5): 1629–1653.

[12] DUNCAN J M, BYRNE P, WONG K S, et al. Strength, stress-strain, and bulk modulus parameters for finite element analyses of stresses and movements in soil masses[R]. Berkeley: College of Engineering, University of California, 1980.

[13] DOMASCHUK L, VALLIAPPAN P. Nonlinear settlement analysis by finite element[J]. Journal of the Geotechnical Engineering Division, ASCE, 1975, 101(7): 601–614.

[14] ZHANG Ji-ru, LUO Ming-xing, PENG Wei-ke, et al. Drained triaxial tests on mechanical properties of calcareous sand under various stress paths[J]. Chinese Journal of Geotechnical Engineering, 2021, 43(4): 593–602.

[15] ZHANG Ji-ru, PENG Wei-ke, ZHENG Yan-jun. Stress-strain model and deformation parameters of K_0-consolidated coral sand[J]. Chinese Journal of Geotechnical Engineering, 2023, 45(3): 478–485.

[16] BIAN Shi-hai, LI Guo-ying, WEI Kuang-min, et al. Study on adaptability of generalized plasticity model of rockfill materials under various stress paths[J]. Hydro-Science and Engineering, 2017(4): 97–104.

[17] MIHAI L A, GORIELY A. How to characterize a nonlinear elastic material? A review on nonlinear constitutive parameters in isotropic finite elasticity[J]. Proceedings of the Royal Society A: Mathematical, Physical and Engineering Sciences, 2017, 473(2207): 1–33.

[18] KONDNER R L. Hyperbolic stress-strain responses: cohesive soils[J]. Journal of the Soil Mechanics and Foundation Division, ASCE, 1963, 89(SM1): 115–143.

[19] LI Xin-ming, KONG Ling-wei, GUO Ai-guo. Stress-strain behavior of expansive soil under K_0 condition with different unloading rates[J]. Rock and Soil Mechanics, 2019, 40(4): 1299–1306.

[20] NIU Xi-rong, YAO Yang-ping, CHEN Zhong-da. The strength and constitutive model of compacted weathered granite soils in Lüliang mountains[J]. Rock and Soil Mechanics, 2017, 38(10): 2833–2840.

[21] XIANG Biao, ZHANG Zong-liang, CHI Shi-chun. Three-modulus incremental nonlinear model of rockfill under paths of constant stress ratio[J]. Chinese Journal of Geotechnical Engineering, 2008, 30(9): 1322–1326.

[22] ZHANG Ji-ru, HUA Chen, LUO Ming-xing, et al. Behavior of particle breakage in calcareous sands during drained triaxial shearing[J]. Chinese Journal of Geotechnical Engineering, 2020, 42(9): 1593–1602.

[23] HARDIN B O. Crushing of soil particles[J]. Journal of Geotechnical Engineering, ASCE, 1985, 111(10): 1177–1192.

[24] GUO P J. Effect of density and compressibility on K_0 of cohesionless soils[J]. Acta Geotechnica, 2010, 5(4): 225–238.

[25] CHU J, GAN C L. Effect of void ratio on K_0 of loose sand[J]. Géotechnique, 2004, 54(4): 285–288.